Multichannel quantum-defect approach for two-photon processes

F. Robicheaux and Bo Gao
Joint Institute for Laboratory Astrophysics, University of Colorado, Boulder, Colorado 80309-0440
(Received 6 July 1992)

We present a method which allows the efficient calculation of the amplitudes for two-photon processes based on variations of the eigenchannel R-matrix method and of the multichannel quantum-defect theory (MQDT). This method contains the flexibility to describe structure due to intermediate- as well as final-state Rydberg series, autoionizing series, and continua. Because the method is based on MQDT, we would be able to describe easily two-photon processes in negative ions as well as in any of the situations previously described by the generalization of MQDT in one-photon processes. We present calculations for two-photon absorption from the ground state of Mg and Ca.

PACS number(s): 32.80.Fb, 32.80.Rm, 32.80.Dz

There has been growing interest in describing multiphoton processes in multielectron atoms [1–11]. The common desire of these studies is to completely and correctly describe the atomic physics while using lowest-order perturbation theory to describe the change in atomic dynamics due to the laser field. In effect, the goal is to develop theoretical tools to describe experiments which use multiphoton processes to probe atomic dynamics usually inaccessible to a one-photon probe. Resonant processes are ruled out due to the use of perturbation theory (weak-field resonant processes are the easiest processes to describe). The major difficulty involved in this problem is the summation over the infinite number of many-electron intermediate states. There are basically two types of approaches to this problem. The first includes various types of L^2-basis techniques [1–6]. The second is to solve the Dalgarno-Lewis differential equation [7,8]. Both methods have had some success in describing processes in which the intermediate photons can probe only up to the first few bound states. It is well known, however, that the differential equation method has the drawback of being unstable near intermediate resonances [7,8] and the L^2-basis techniques are cumbersome to use if one of the intermediate photons can put the system into the continuum [above-threshold ionization (ATI) processes] [9]. Furthermore, neither of these methods is suitable in practice for describing processes in which the intermediate photons can put the electrons right in a high Rydberg series where the fast variation of cross sections as a function of energy can only be described by applying multichannel quantum-defect theory (MQDT) to the effective *intermediate* states. Such an application of MQDT has already been proposed by Fink and Zoller [11]. This paper describes how to wed their procedure to *ab initio* calculations obtaining a procedure as accurate as those of previous workers but without some of the constraints imposed by the L^2-basis technique.

The method for calculating two-photon processes which we will describe in this paper was chosen to exploit the power and stability of computer codes used for atomic photoionization. Namely, we have adapted the eigenchannel R-matrix techniques of Greene and co-workers to this problem [12]. We also utilize the adaptation of MQDT that Fink and Zoller [11] have described for two-photon processes. It is well known that the combination of these two procedures (R-matrix and MQDT) provides accurate, stable, and efficient *ab initio* calculations of atomic photoionization. We show how these two approaches can be linked to provide an accurate and automated approach to two-photon processes. The possibility of using (Wigner-Eisenbud) R-matrix techniques to solve the Dalgarno-Lewis differential equation has already been discussed and implemented [10] but only when the first photon cannot excite the atom to large distances. We circumvent this difficulty by using MQDT for the Dalgarno-Lewis function. A brief report of this investigation has been given elsewhere [13].

INHOMOGENEOUS SOLUTION

The two-photon amplitude for going from state Ψ_0 to state Ψ_f is

$$T^{(2)}_{f\leftarrow 0}=\sum\int d\varepsilon\langle\Psi_f|D|\varepsilon\rangle(E_0+\omega-\varepsilon+i\eta)^{-1}\langle\varepsilon|D|\Psi_0\rangle\ ,\quad \eta\rightarrow 0+\ , \tag{1}$$

where D is the dipole operator (we will always use the length gauge) and ω is the laser frequency. We solve Eq. (1) by the procedure of Dalgarno and Lewis [14], setting $T^{(2)}_{f\leftarrow 0}=\langle f|D|\Lambda_p\rangle$, with Λ_p the solution of the inhomogeneous equation

$$(E-H)\Lambda_p=D\Psi_0\ , \tag{2}$$

where $E=E_0+\omega$ and the limit $\eta\rightarrow 0+$ in Eq. (1) translates to imposing outgoing-wave boundary conditions on Λ_p in the open channels. Λ_p is the physically relevant inhomogeneous solution; for ease of calculation we will introduce other solutions of (2) with different asymptotic boundary conditions. Ψ_0 is the initial-state wave function.

Equation (2) is ripe for a MQDT-type treatment: all of the complicated dynamics occur in a small region near the nucleus. In this spirit we solve Eq. (2) disregarding

the boundary conditions at large distances from the nucleus. This solution, which we denote Λ_s, will diverge in the closed channels and have nonzero amplitude for incoming waves in the open channel. We obtain the solution of (2) which has the correct boundary conditions by adding to Λ_s a finite amount of the homogeneous solution ψ_j, which we calculate from

$$(E-H)\psi_j=0 . \tag{3}$$

We write the solution of Eq. (2) which has the correct boundary conditions as $\Lambda_p=\Lambda_s+\sum_j\psi_j A_j$, where the summation over j is from 1 to N, with N being the number of channels included in the calculation. The A_j are determined by an inhomogeneous matrix equation containing information on the boundary conditions on Λ_p. We will describe this matrix equation in the next section.

MQDT FOR THE INHOMOGENEOUS FUNCTION

The solution of Eq. (2) has particular boundary conditions. Namely, Λ_p is finite everywhere and, for the channels in which the electron can escape, Λ_p can only have outgoing waves (this condition arises from $\eta\rightarrow 0+$). The structure of Eq. (2) implies that its solution is ripe for a MQDT-type treatment. All of the complicated dynamics are concentrated at short range while the long-range force felt by the electron has a simple form and thus its dynamics is subject to analytic treatment. The MQDT parameters vary slowly with energy because the forces near the nucleus, where the complicated dynamics take place, are strong. The possibility of adapting these ideas to the Dalgarno-Lewis function Λ_p was first discussed by Fink and Zoller [11]; in this section we rederive their results from a slightly different viewpoint and with different notation. Before describing the adaptation of MQDT to the inhomogeneous problem, we give a brief account of the ideas and notation for applying the usual MQDT ideas for the wave function.

Outside of a core region, the potential is almost purely $-Z/r$ and it is possible to describe the wave function using only a small number of parameters which only have a slight energy dependence. This is possible because the complicated dynamics near the core is dominated by large field gradients while only a few angular momenta are relevant. For an N-channel problem we can write the N linearly independent wave functions as [15]

$$\psi_k=\mathcal{A}\sum_j\phi_j[f_j(r)\delta_{jk}-g_j(r)K_{jk}], \quad r>r_c , \tag{4}$$

where K_{jk} is the real-symmetric reacting matrix, $\mathcal{A}$ is the antisymmetrization operator which has no practical effect since the electrons are in different regions of space, and ϕ_j are the target functions which depend on all of the variables except the outer electron's radius. E_j is the amount of energy in the target function ϕ_j and thus the amount of energy available to the outer electron in channel j is $\varepsilon_j=E-E_j$. The power of MQDT comes from the realization that Eq. (4) is true even for the closed channels, (i.e., those with $E<E_j$) whose f_j and g_j are diverging at $r\rightarrow\infty$. The f_j and g_j are the solutions of the radial Schrödinger's equation with a Coulomb potential which are regular and irregular (respectively) at $r\rightarrow 0$. The asymptotic forms of f_j and g_j are known analytically,

$$f_j(r)\rightarrow\sqrt{2/k_j\pi}\sin\left[k_jr+\frac{Z}{k_j}\ln r+\eta_j\right] , \tag{5}$$

$$g_j(r)\rightarrow-\sqrt{2/k_j\pi}\cos\left[k_jr+\frac{Z}{k_j}\ln r+\eta_j\right] \tag{6}$$

for the open channels $E-E_j=k_j^2/2\geq 0$, and

$$f_j(r)\rightarrow[(D^{-1}r^{-Z/\kappa_j}e^{\kappa_j r})\sin\beta_j -(Dr^{Z/\kappa_j}e^{-\kappa_j r})\cos\beta_j]/\sqrt{\pi\kappa_j} , \tag{5'}$$

$$g_j(r)\rightarrow-[(D^{-1}r^{-Z/\kappa_j}e^{\kappa_j r})\cos\beta_j +(Dr^{Z/\kappa_j}e^{-\kappa_j r})\sin\beta_j]\sqrt{\pi\kappa_j} \tag{6'}$$

for the closed channels $E-E_j=-\kappa_j^2/2\leq 0$. The important parameter for the closed channels is the ratio $f_j/g_j\rightarrow-\tan\beta_j$ as $r\rightarrow\infty$. In these equations Z is the charge of the ion and the phase parameters η_j [of Eqs. (5) and (6)] and β_j [of Eqs. (5') and (6')] depend on the energy as

$$\eta_j=\frac{Z}{k_j}\ln(2k_j)-\frac{l_j\pi}{2}+\arg\Gamma\left[l+1-\frac{iZ}{k_j}\right] , \tag{7}$$

$$\beta_j=\pi(Z/\kappa_j-l_j) . \tag{8}$$

All of the rapid energy dependence evolves from superposing the different ψ_j so that the resulting functions converge to zero at large distances in the closed channels. Another important point is that the dipole matrix elements of the functions Eq. (4), $\langle\psi_j|D|\Psi_0\rangle$, also vary slowly with energy because Ψ_0 is limited to a restricted region of space near the nucleus.

We now describe how to apply these ideas to the inhomogeneous solution of Eq. (2). Outside the core region, the right-hand side of Eq. (2) is exponentially small and can be set to zero without introducing any practical errors. Therefore Λ_p has the same form as the homogeneous function in this region of space because at $r\geq r_c$ they solve the same differential equation. We express Λ_p as

$$\Lambda_p=\mathcal{A}\sum_j\phi_j[f_j(r)\lambda_{jp}^{(f)}-g_j(r)\lambda_{jp}^{(g)}], \quad r\geq r_c . \tag{9}$$

In the open channels Λ_p must go asymptotically to $\exp(ik_jr)$. We substitute Eqs. (5) and (6) into Eq. (9) and find the coefficient of the $\exp(-ik_jr)$ term to be $i\lambda_{jp}^{(f)}+\lambda_{jp}^{(g)}$, which must be set equal to zero. Similarly, for the closed channels we substitute Eqs. (5') and (6') into Eq. (9) and find that for Λ_p to converge at large distances then $\lambda_{jp}^{(f)}\sin\beta_j+\lambda_{jp}^{(g)}\cos\beta_j=0$ in all of the closed channels. These two sets of equations *completely* determine Λ_p.

The best way to obtain the solution to Eq. (2) with the correct boundary conditions is to use *any* solution of Eq. (2) (which in general will not have the correct boundary

conditions) and then add to it a finite amount of the homogeneous solutions. By modifying the coefficients of the homogeneous solutions we can obtain the correct boundary conditions. Specifically,

$$\Lambda_p=\Lambda_s+\sum_j \psi_j A_j \ , \tag{10}$$

where Λ_s is a solution of Eq. (2) with unphysical boundary conditions. Λ_s does not usually vary rapidly with energy. It has the asymptotic form

$$\Lambda_s=\mathcal{A}\sum_j \phi_j(f_j\lambda_{js}^{(f)}-g_j\lambda_{js}^{(g)}) \ . \tag{11}$$

From Eqs. (10) and (11) it is easy to see that $\lambda_{jp}^{(f)}=\lambda_{js}^{(f)}+A_j$ and $\lambda_{jp}^{(g)}=\lambda_{js}^{(g)}+\sum_k K_{jk}A_k$. We now apply the boundary conditions

$$\tan\beta_j\lambda_{jp}^{(f)}+\lambda_{jp}^{(g)}=0 \tag{12a}$$

if j is a closed channel

$$i\lambda_{jp}^{(f)}+\lambda_{jp}^{(g)}=0 \tag{12b}$$

if j is an open channel

to obtain the inhomogeneous matrix equation for the coefficients A,

$$\mathbf{A}=-(\underline{K}+\underline{B})^{-1}(\lambda_s^{(g)}+\underline{B}\lambda_s^{(f)}) \ , \tag{13}$$

where $\underline{B}$ is a diagonal matrix with components $\tan\beta_j$ if the j channel is closed and $i=\sqrt{-1}$ if the j channel is open. $\underline{B}$ contains all of the rapid energy dependence resulting from the application of boundary conditions at large distances. Note that $\mathbf{A}$ diverges when $\det(\underline{K}+\underline{B})=0$. This possibility only arises when all of the intermediate-state channels are closed; the zeroes are exactly at the bound-state energies of the intermediate state.

These equations are exact, but in a sense the Λ_s are not very useful for interpolation. In the usual MQDT the important parameters are practically energy independent over large ranges of energy due to the strong forces near the nucleus [15]. For our case it is true for the homogeneous solution, but it is meaningless to interpolate the parameters which depend upon the inhomogeneous solution Λ_s since it is *any* solution of Eq. (2). So for the purposes of interpolation we define boundary conditions for Λ_s that do not depend on whether the channel is open or closed at large distances but will be sufficient to completely determine Λ_s. A standard parameterization also facilitates the characterization of the dynamics.

We choose the smooth inhomogeneous function to have outgoing waves in *all* of the channels, whether open or closed. By outgoing waves in closed channels we mean the solution $f+ig$. The resulting Λ_s has the asymptotic form

$$\Lambda_s=\mathcal{A}\sum_j \phi_j(f_j+ig_j)\lambda_{js} \ . \tag{14}$$

Consequently, Eq. (13) for $\mathbf{A}$ reduces to

$$\mathbf{A}=-(\underline{K}+\underline{B})^{-1}(i+\underline{B})\lambda_s \ . \tag{13'}$$

This choice is consistent with the philosophy of MQDT, which treats all channels as open until a later step, where one analytically closes the channels for which the electron has negative kinetic energy.

R MATRIX FOR THE INHOMOGENEOUS FUNCTION

It is obvious that Eq. (2) can be solved by slightly modifying any of the standard *ab initio* techniques of atomic physics. Our familiarity with the eigenchannel R-matrix procedures leads us to adapt that method to our purposes. We also have great confidence in its accuracy dating from the success it has produced in photoionization calculations of complicated atoms [12]. We will show that the inhomogeneous R-matrix equation can be streamlined using the same methods as Ref. [16] to facilitate calculations.

The eigenchannel R matrix is a variational principle for the logarithmic derivative of the wave function at the reaction surface. We look for exact wave functions at a fixed energy which have constant normal derivatives satisfying $\partial\psi_E/\partial n+b(E)\psi_E=0$. The R-matrix equation for $b(E)$ is

$$b(E)\int dS\,\psi_t^2=2\int dV\,\psi_t(E-H)\psi_t-\int dS\,\psi_t\frac{\partial\psi_t}{\partial n} \ , \tag{15}$$

where $\psi_t=\psi+\delta$. In practice ψ_t is expanded in a linear superposition of basis functions y_j, not all of which have the same logarithmic derivative on the boundary. The variational procedure becomes a matrix equation of the generalized eigenvalue type [12]

$$b_{\beta\underline{\sigma}}\mathbf{C}_\beta=\underline{\Gamma}\mathbf{C}_\beta \ , \tag{16}$$

where

$$\Gamma_{kj}=2\int dV\,y_k(E-H)y_j-\int dS\,y_k\frac{\partial y_j}{\partial n} \tag{17}$$

and

$$\sigma_{kj}=\int dS\,y_k y_j \ . \tag{18}$$

The symbol $\int dV$ indicates integration over the R-matrix volume, which is usually defined to be $r_i\le r_c$ (i.e., all electrons confined to radii distances less than r_c), and $\int dS$ indicates integration over the surface of the R-matrix volume. Equation (16) determines b and $\mathbf{C}$ and thus the value and derivative of the wave function at the reaction surface: $\psi(r_c)=\sum_j C_j y_j$ and $\psi'(r_c)=-b\psi(r_c)$. The eigenchannel R matrix works well for both single-channel and multichannel situations.

For the inhomogeneous function the variational principle for the logarithmic derivative is meaningless. This difficulty arises because it is always possible to add some of the homogeneous solution to Λ_t, spoiling the variational properties. The analog of Eq. (16) that we use for $\Lambda=\sum_j y_j C_{j\lambda}$ is

$$(\underline{\Gamma}-b_\lambda\underline{\sigma})\mathbf{C}_\lambda=2\mathbf{Z} \ , \tag{19}$$

where $Z_j=\langle y_j|D|\Psi_0\rangle$ and Γ and σ are as defined in Eqs. (17) and (18). The value and derivative of Λ at the R-matrix boundary are $\Lambda(r_c)=\sum_j y_j(r_c)C_{j\lambda}$ and $\partial\Lambda(r_c)/\partial n=-b_\lambda\Lambda(r_c)$. Equation (9) has two unknowns: b_λ and $\mathbf{C}_\lambda$. In practice we obtain a solution to Eq. (19) by choosing an arbitrary b_λ giving $\mathbf{C}_\lambda=2(\underline{\Gamma}-b_\lambda\underline{\sigma})^{-1}\mathbf{Z}$. Any b_λ will suffice as long as $(\underline{\Gamma}-b_\lambda\underline{\sigma})^{-1}$ is nonsingular. Because we also use the homogeneous solution, we first solve Eq. (16) to obtain b_β and $\mathbf{C}_\beta$; we only need to choose b_λ different from all of the b_β's to make $\mathbf{C}_\lambda$ finite.

Equation (19) can be streamlined in a manner similar to the procedure of Ref. [16]. The basis functions $y_j^{(c)}$ are called closed if $y_j^{(c)}(r_c)=0$ and open otherwise. As in Ref. [16], the closed functions are automatically orthogonal to each other and the open functions are Gramm-Schmidt orthogonalized to the closed-type functions and each other. We order the basis functions so that the functions 1 to N_c are the closed type and the functions N_c+1 to $N_c+N_o=N_{\rm tot}$ are the open type. We now label the Γ matrix by blocks

$$\underline{\Gamma}=\begin{bmatrix}\underline{\Gamma}^{cc} & \underline{\Gamma}^{co}\\ \underline{\Gamma}^{oc} & \underline{\Gamma}^{oo}\end{bmatrix} \tag{20}$$

and similarly for $\underline{\sigma}$, $\mathbf{C}$, and $\mathbf{Z}$. In the matrix $\underline{\sigma}$, only the block $\underline{\sigma}^{oo}$ is nonzero. We now rewrite (19) as two equations:

$$(\underline{\Gamma}^{oo}-b_\lambda\underline{\sigma}^{oo})\mathbf{C}_\lambda^o+\underline{\Gamma}^{oc}\mathbf{C}_\lambda^c=2\mathbf{Z}^o\,, \tag{21}$$

$$\underline{\Gamma}^{co}\mathbf{C}_\lambda^o+\underline{\Gamma}^{cc}\mathbf{C}_\lambda^c=2\mathbf{Z}^c\,. \tag{21'}$$

We solve Eq. (21') for $\mathbf{C}_\lambda^c$ and then substitute $\mathbf{C}_\lambda^c$ into (21) to obtain

$$\mathbf{C}_\lambda^c=-[\underline{\Gamma}^{cc}]^{-1}(\underline{\Gamma}^{co}\mathbf{C}_\lambda^o-2\mathbf{Z}^c)\,, \tag{22}$$

$$(\underline{\Gamma}^{oo}-\underline{\Gamma}^{oc}[\underline{\Gamma}^{cc}]^{-1}\underline{\Gamma}^{co}-b_\lambda\underline{\sigma}^{oo})\mathbf{C}_\lambda^o =2(\mathbf{Z}^o-\underline{\Gamma}^{oc}[\underline{\Gamma}^{cc}]^{-1}\mathbf{Z}^c)\,. \tag{23}$$

Although these equations do not appear to be a big improvement over Eq. (19), they really allow the practical implementation of the R-matrix method. This is because $\underline{\Gamma}^{cc}=2(\underline{E}-\underline{H}^{cc})$; by using closed basis functions which diagonalize $\underline{H}^{cc}$ (this diagonalization needs to be carried out only once), inverting $\underline{\Gamma}^{cc}$ becomes trivial because it is diagonal. The number of open basis functions is usually about an order of magnitude smaller than the number of closed basis functions, which means it is *much* faster to solve Eq. (23) than Eq. (19).

The resulting inhomogeneous function Λ_r is real everywhere and therefore does not correspond to the inhomogeneous function Λ_s of Eq. (14). For purposes of interpolation we need to convert Λ_r to Λ_s by adding to it some of the homogeneous solution. The asymptotic form of Λ_r is $\Lambda_r=\sum_j\phi_j(f_j\lambda_{jr}^{(f)}-g_j\lambda_{jr}^{(r)})$. We find

$$\Lambda_s=\Lambda_r-\sum_{j,k}\psi_j(\underline{K}+i)_{jk}^{-1}(\lambda_{kr}^{(g)}+i\lambda_{kr}^{(f)})\,. \tag{24}$$

The λ_{js} are

$$\lambda_s=\tfrac{1}{2}[\lambda_r^{(f)}+\lambda_r^{(g)}-i(\underline{K}-\underline{i})(\underline{K}+\underline{i})^{-1}(\lambda_r^{(g)}+i\lambda_r^{(f)})]\,. \tag{25}$$

We would now like to repeat the point made above. The Λ_s and λ_s are useful only in the MQDT sense; they do not vary rapidly with energy and are therefore useful for the purpose of interpolation and for parameterizing the dynamics near the nucleus. For atoms which are LS coupled, we do not need to worry about interpolation because the streamlined R-matrix calculation, Eqs. (19)–(23), is fast enough that we can calculate Λ at thousands of energy points.

CROSS SECTIONS AND ANGULAR RECOUPLING

In all that follows, we will focus on the formulas relevant for atomic dynamics in LS coupling; we completely ignore spin-orbit effects. It appears to be straightforward to incorporate spin-orbit effects for atoms as heavy as Ba by applying the LS-to-jj frame transformation to the Λ_s of Eq. (14). However, the resulting formulation of multiphoton absorption for jj-coupled atoms is complicated and beyond the scope of this paper.

To get the total cross section from Eq. (1), one needs to sum over the magnetic quantum numbers m_f and m_i. Explicitly, we have

$$\sum_{L_f}\sum_{m_f,m_0}|T_{f\leftarrow 0}^{(2)}|^2=\sum_{L_f,L_I,L_I'}D(L_fL_I)D^*(L_fL_I')P_{q'q}(L_fL_IL_I'L_0)\,, \tag{26}$$

where

$$D(L_fL_I)=\langle\psi_f(L_f)||D||\Lambda_p(L_I)\rangle =\sum\int d\varepsilon\langle\Psi_f||D||\varepsilon\rangle(E_0+\omega-\varepsilon+i\eta)^{-1}\langle\varepsilon||D||\Psi_0\rangle,\ \ \eta\to 0+ \tag{27}$$

is the reduced dipole matrix element between the final state of angular momentum L_f and the inhomogeneous function of angular momentum L_I and $P_{qq'}$ contains the dependence on the polarization and is the summation of four 3-j coefficients over all magnetic quantum numbers:

$$P_{q'q}(L_fL_IL_I'L_0)=-1^{L_I+L_I'}\sum_{\text{all }m}\begin{pmatrix}L_f & 1 & L_I\\ -m_f & q' & m_I\end{pmatrix}\begin{pmatrix}L_I & 1 & L_0\\ -m_I & q & m_0\end{pmatrix}\begin{pmatrix}L_f & 1 & L_I'\\ -m_f & q' & m_I'\end{pmatrix}\begin{pmatrix}L_I' & 1 & L_0\\ -m_I' & q & m_0\end{pmatrix}. \tag{28}$$

In Eqs. (26)–(28), q, is the polarization of the first absorbed photon and q' is the polarization of the second absorbed

photon. For most experiments $q=q'$; $q(q')=0$ for linearly polarized light. Equation (28) can be reduced to

$$(-1)^{-s}P_{q'q}=\frac{1}{3}\begin{Bmatrix}0 & 1 & 1\\ L_f & L_I' & L_I\end{Bmatrix}\begin{Bmatrix}0 & 1 & 1\\ L_0 & L_I' & L_I\end{Bmatrix}-\frac{qq'}{2}\begin{Bmatrix}1 & 1 & 1\\ L_f & L_I' & L_I\end{Bmatrix}\begin{Bmatrix}1 & 1 & 1\\ L_0 & L_I' & L_I\end{Bmatrix}$$
$$+\tfrac{1}{6}(3q^2-2)(3q'^2-2)\begin{Bmatrix}2 & 1 & 1\\ L_f & L_I' & L_I\end{Bmatrix}\begin{Bmatrix}2 & 1 & 1\\ L_0 & L_I' & L_I\end{Bmatrix}, \tag{29}$$

where $s=L_0+L_I+L_I'+L_f$ by using Eq. (6.2.8) of Ref. [17]. None of the operations $q\leftrightarrow q'$, $L_0\leftrightarrow L_f$, or $L_I\leftrightarrow L_I'$ change $P_{qq'}$. For unpolarized light, we average over right- and left-handed circularly polarized light to obtain

$$(-1)^{-s}P_u=\frac{1}{3}\begin{Bmatrix}0 & 1 & 1\\ L_f & L_I' & L_I\end{Bmatrix}\begin{Bmatrix}0 & 1 & 1\\ L_0 & L_I' & L_I\end{Bmatrix}+\frac{1}{6}\begin{Bmatrix}2 & 1 & 1\\ L_f & L_I' & L_I\end{Bmatrix}\begin{Bmatrix}2 & 1 & 1\\ L_0 & L_I' & L_I\end{Bmatrix}. \tag{30}$$

The total generalized cross section can now be compactly expressed as

$$\frac{\sigma^{(2)}}{I}=\frac{5.7466\times10^{-35}\omega}{2L_0+1}\sum_{L_f,L_I,L_I'}D(L_fL_i)D^*(L_fL_I')P(L_fL_IL_I'L_0)\ \ (\mathrm{cm^4\,W^{-1}}), \tag{31}$$

where ω is the laser frequency in atomic units, the reduced dipole matrix elements D are also in atomic units, and where P can be obtained from Eqs. (29) or (30), depending on whether or not the light is polarized. To obtain the measured cross section in units of $\mathrm{cm^2}$ multiply Eq. (31) by the laser intensity in units of $\mathrm{W/cm^2}$.

REDUCED DIPOLE MATRIX ELEMENTS

The calculation of the reduced dipole matrix element of Eq. (27) can be accomplished by dividing it into three steps. The first part of the calculation restricts all of the radii to distance less than the R-matrix box radius. This piece is calculated numerically and we call it $D(L_f,L_I)_{\mathrm{box}}$. There are two contributions to the reduced dipole matrix element when one of the electrons is outside of the box; there is no contribution to the dipole matrix element when two electrons are outside of the box because the wave function is assumed to be zero in this case.

One contribution to the dipole matrix element (when one of the particles is outside the R-matrix volume) consists of the dipole matrix elements between core states multiplied by the overlap of Coulomb functions outside the box:

$$D(L_f,L_I)_{\mathrm{out},1}=(-1)^{L_I+1}\delta_{S_I,S_f}[L_f][L_I]\sum_{i,j}(-1)^{L_c^i+l^i}\langle\phi_i||D||\phi_j\rangle\delta_{l^jl^i}\begin{Bmatrix}L_c^i & L_f & l^i\\ L_I & L_c^j & 1\end{Bmatrix}$$
$$\times\int_{r_c}^{\infty}dr(f_{\omega+\varepsilon_i}I_{if}-g_{\omega+\varepsilon_i}J_{if})(f_{\varepsilon_j}\lambda_{jp}^{(f)}-g_{\varepsilon_j}\lambda_{jp}^{(g)}), \tag{32}$$

where L_c^j is the total orbital angular momentum of the core state ϕ_j in Eqs. (33), the symbol $[L]=\sqrt{2L+1}$, and where outside the R-matrix volume

$$\Lambda_p(L_I)=\sum_i(\phi_iY_{l^i})^{L_I}[f_{\varepsilon_i,l^i}(r)\lambda_{ip}^{(f)}-g_{\varepsilon_i,l^i}(r)\lambda_{ip}^{(g)}],\quad r>r_c \tag{33a}$$

$$\psi_f(L_f)=\sum_i(\phi_iY_{l^i})^{L_f}[f_{\varepsilon_i+\omega,l^i}(r)I_{if}-g_{\varepsilon_i+\omega,l^i}(r)J_{if}],\quad r>r_c, \tag{33b}$$

with $\varepsilon_i=E_0+\omega-E_i$. The symbol $(\phi_iY_{l^i})^{L_I}$ is meant to indicate that the total orbital angular momentum of the core state i, L_c^i, is coupled to the orbital angular momentum l^i of the outer electron to give total orbital angular momentum L_I. Finally, S is the total spin, which cannot change during photoabsorption processes (if the atom is LS coupled). The geometric (6-j) factor results from the uncoupling of the angular momentum of the core from the angular momentum of the outer electron. This operation is necessary to obtain the matrix element of a tensor operator which only acts on a piece of the wave function. This is a well-known relationship found in any of the books on angular momentum [e.g., Eq. (7.1.7) of Ref. [17]]. This contribution to the dipole matrix element is essentially the same as the total transition matrix element probed by isolated core experiments [18].

Special difficulties arise when $\omega=|E_i-E_j|$, i.e., when $\omega+\varepsilon_i=\varepsilon_j$ in Eq. (32). In this case, the overlap of the Coulomb functions increases rapidly as ε_j approaches 0 from below and diverges when $\varepsilon_j\geq0$. This divergence occurs because we are not even close to correctly describing the physics using perturbation theory. When $\omega\sim|E_i-E_j|$, the core states should be a dressed mixture of ϕ_i and ϕ_j. Interesting physics occurs where the per-

turbation theory breaks down. A possible two-color experiment might be to tune a strong laser to a dipole-allowed transition of the *core* and scan the frequency of the second (weaker probe) laser near the thresholds of the dressed core states. The coupling between the dressed channels can be controlled through the choice of intensity *and* detuning of the first strong laser. Wang and Greene [19] have discussed the qualitative evolution of the spectra of interacting channels when one has one tunable parameter available; experimentally, the detuning of a laser can be controlled better than the intensity.

The other contribution to the dipole matrix element (when one of the particles is outside of the R-matrix volume) consists of the overlap matrix elements between core states multiplied by the dipole integral of Coulomb functions outside the box:

$$D(L_f,L_I)_{\text{out},2}=(-1)^{L_f+1}[L_f][L_I]\sum_{i,j}(-1)^{L_c^i+l^j+l^i}[l^i][l^j]\langle\phi_i|\phi_j\rangle\begin{Bmatrix} l^i & L_f & L_c^i \\ L_I & l^j & 1\end{Bmatrix}\begin{bmatrix} l^i & 1 & l^j \\ 0 & 0 & 0\end{bmatrix}$$
$$\times\int_{r_c}^{\infty}dr(f_{\varepsilon_i+\omega}I_{if}-g_{\varepsilon_i+\omega}J_{if})r(f_{\varepsilon_j}\lambda_{ip}^{(f)}-g_{\varepsilon_j}\lambda_{ip}^{(g)})\ . \tag{34}$$

The geometric (six-j) factor arises from the same sort of recoupling described above [see Eqs. (33) above and Eq. (7.1.8) in Ref. [17]], while the 3-j factor stems from the reduced matrix element of $Y_1 m$. Equation (34) represents photoabsorption by the continuum electron outside of the R-matrix volume. Essentially, this gives the amplitude for the outer electron to absorb a photon leaving the core unchanged. The integral over the Coulomb functions present special difficulties when in the continuum.

In both $D(L_f,L_I)_{\text{out}}$ elements, we must evaluate integrals from r_c to infinity of the product of two Coulomb functions. These integrals cannot be evaluated in a brute force manner if we hope to evaluate then quickly and efficiently. To evaluate these integrals, we use an asymptotic expansion. To see how we generate the terms of this expansion, we introduce two generic functions F_1 and F_2, which are solutions of different Schrödinger's equations; $F_i''=-2(E_i-V_i)F_i$ or $H_iF_i=E_iF_i$, where $2H_i=-\partial^2/\partial r^2+2V_i(r)$. The first useful relationship is

$$\bar{\omega}F_1F_2=-\tfrac{1}{2}(F_1'F_2-F_1F_2')'\ , \tag{35}$$

where $\bar{\omega}=E_1-E_2-V_1+V_2$. The second relationship is more complicated but crucial to the evaluation of the Coulomb integrals:

$$\bar{\omega}(F_1'F_2-F_1F_2')=\tfrac{1}{2}(F_1F_2)'''+2[(E_1-V_1+E_2-V_2)F_1F_2]'+(V_1+V_2)'F_1F_2\ . \tag{35'}$$

Equations (35) and (35') are both generated in the same manner; for example, $(E_1-E_2)F_1'F_2=(H_1F_1)'F_2-F_1'(H_2F_2)$. The asymptotic series can be generated in a straightforward manner from Eqs. (35); for example, we can use Eq. (35) to find the integral of F_1F_2 multiplied by any function G in terms of the derivative of G and the Wronskian of F_1 and F_2 as

$$\int_{r_0}^{r_f}F_1F_2G\,dr=-\tfrac{1}{2}\int_{r_0}^{r_f}(G/\bar{\omega})(F_1'F_2-F_1F_2')'dr\ . \tag{36}$$

Integrate the right-hand side of Eq. (36) by parts to obtain the integral of F_1F_2G as a sum of surface terms and an integral of a new function $(G/\bar{\omega})'$ multiplied by $F_1'F_2-F_1F_2'$. We use Eq. (35') for this new integral, again integrating by parts to obtain surface terms and a new integral (whose integrand is a function multiplied by F_1F_2). This procedure can be repeatedly iterated; however, after a few iterations the surface terms begin to grow with each iteration so that the series we obtain is strictly an asymptotic series. When we use this procedure to determine the integrals in Eqs. (32) and (34) we set the terms from the upper limit of integration (i.e., $r\to\infty$) equal to zero. The resulting solution works when $|l^j(l^j+1)-l^i(l^i+1)|\ll 2\omega r_c^2$ and $2\omega^2 r_c^3\gg 1$. For two-photon processes and neutral atomic systems these restrictions are always satisfied because when ω is too small to satisfy these restrictions it is also too small to excite an electron to distances larger than the R-matrix radius; in this case, Λ_p is very nearly zero outside of the reaction zone. This procedure is very efficient where it can be applied because each term in the expansion involves F_i and its first derivative [which are needed anyway to determine Eqs. (33)] and simple functions of r_c.

RESULTS

In Figs. 1–6 we plot our calculated two-photon cross sections for Mg and Ca as a function of laser frequency. Our calculations agree with previous calculations within the 50% we could read off the previous results; the shapes are also in good agreement. In all of these plots

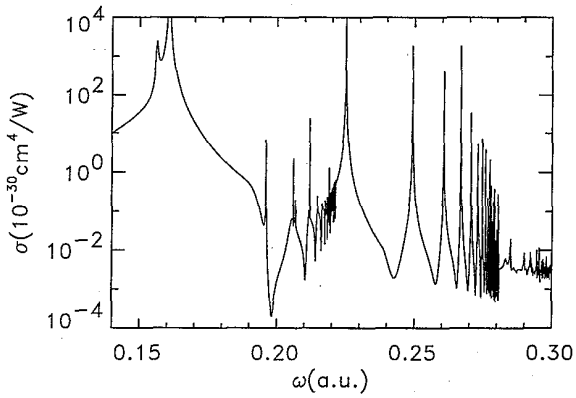

FIG. 1. Total two-photon ionization cross section for Mg from threshold to just above the frequency needed for one-photon ionization. ω is the frequency of the laser which is assumed to be linearly polarized.

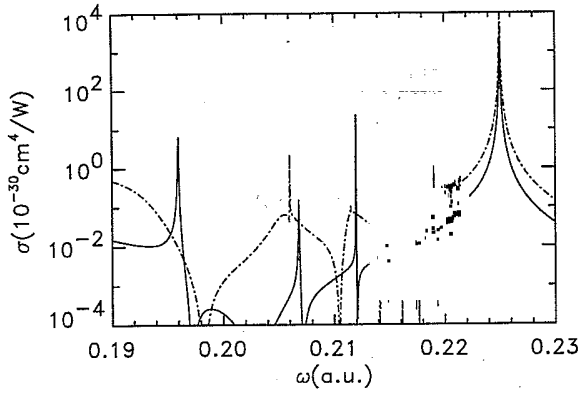

FIG. 2. ^1S (solid line) and ^1D (dot-dashed line) contribution to the total two-photon ionization cross sections. The Rydberg series are final-state autoionizing resonances attached to the $3p$ threshold.

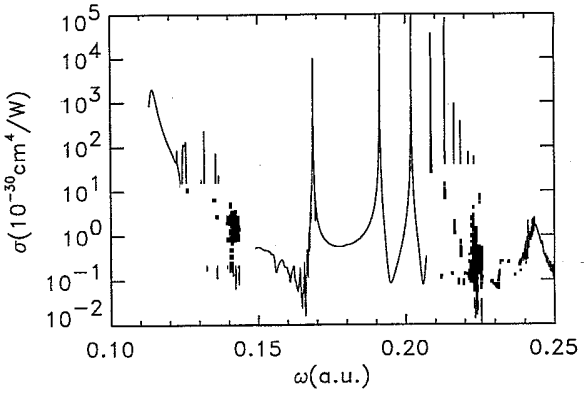

FIG. 4. Same as Fig. 1, except for Ca.

we assume that both absorbed photons are linearly polarized in the same direction. The ground state of these atoms is $ns^2\,^1S$ (with $n=3$ for Mg and 4 for Ca), which means the intermediate states can only have $^1P^o$ symmetry; $L_I=1$. The final state can have ^1S or ^1D symmetry [$^1P^e$ symmetry is forbidden for two linearly polarized photons, see Eq. (28)]; $L_f=0$ or 2. In Figs. 2 and 5 we plot the ^1S and ^1D contributions to the total cross section separately to show that at most energies the ^1D symmetry dominates the total cross section.

One striking difference between one- and two-photon cross sections is the overpowering role played by resonances; there is essentially *no* continuum background for two-photon ionization. This fact is not obvious when the cross section is plotted on a log scale and may explain the lack of enthusiasm for experimental studies of *nonresonant* multiphoton ionization. Another difference is that Rydberg series of resonances can arise during the absorption of the first or second photon; however, it is usually fairly easy to disentangle these effects. For example, in Fig. 1 the Rydberg series attached to the threshold at $\omega\sim0.28$ a.u. is from the $3snp\ ^1P^o$ intermediate-state resonances of Mg, while in Fig. 4 the Rydberg series attached to the threshold at $\omega\sim0.22$ a.u. is from the $4snp\ ^1P^o$ intermediate-state symmetry of Ca. All of the other Rydberg series of resonances are from the even-symmetry final-state autoionizing resonances.

In Figs. 1–3 we plot the two-photon ionization cross section of Mg. The spectrum plotted in Fig. 1 is not very interesting; almost all of the visible structures above 10^{-30} cm^{14}/W are due to the $3snp\ ^1P^o$ intermediate state resonances. In Fig. 2 we show a blowup of the ^1S and ^1D cross sections between the $3s3p\ ^1P^o$ and $3s4p\ ^1P^o$ intermediate-state resonances. There are three clear autoionizing series; they have the character $3pnp\ ^1S$ (solid line), $3pnp\ ^1D$, and $3pnf\ ^1D$. The $3pnp\ ^1S$ series is sharp because it can only decay to the $3s\varepsilon s\ ^1S$ continuum, which is propensity unfavored [19]. The other sharp autoionizing series is the $3pnf\ ^1D$, which has a hard time decaying because it can only decay to the $3s\varepsilon d\ ^1D$ continuum, which is propensity unfavored (in fact, these resonances are so narrow only the lowest one at $\omega=0.206$ a.u. can be clearly seen). The broad series is the $3pnp\ ^1D$, which quickly decays to the $3s\varepsilon d\ ^1D$ continuum. In Fig. 3 we show a blowup of the region near $\omega\sim0.16$ a.u. The autoionizing resonance shown here is the $3p^2\,^1S$ resonance. This region was studied experimentally by Bonnano, Clark, and Lucatorto [20]; they were able to observe this resonance. The position of our resonance was only slightly shifted from the measured position. The calculated shape did not match the experimental

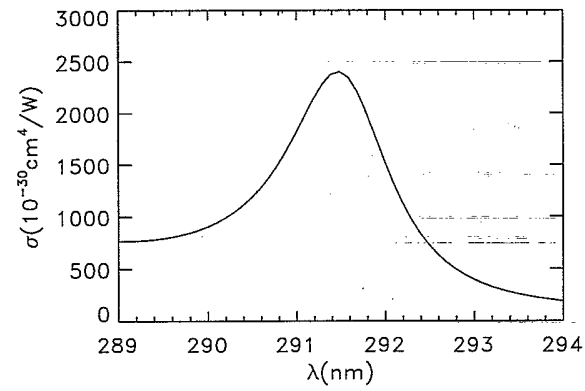

FIG. 3. Total two-photon ionization cross section as a function of laser wavelength. The resonance is from the $3p^2\,^1S$ autoionizing state.

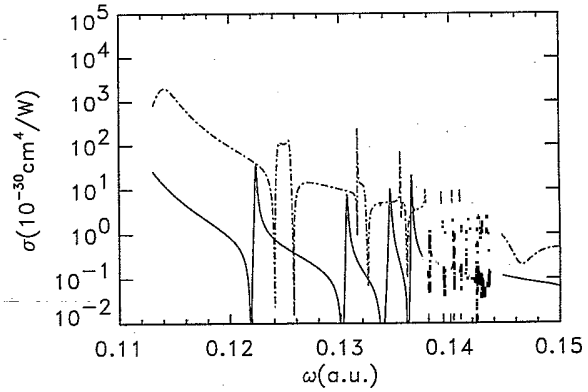

FIG. 5. Same as Fig. 2, except the Rydberg series are attached to the $3d$ threshold of Ca.

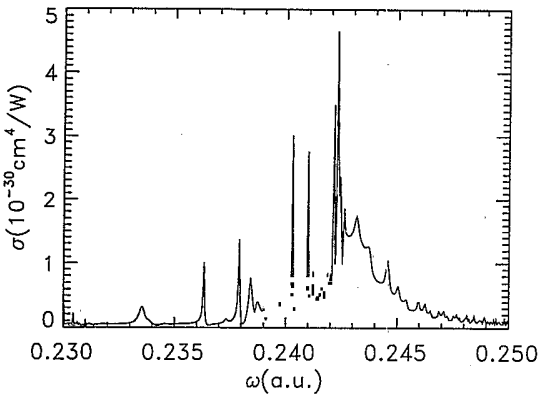

FIG. 6. Total two-photon ionization cross section near the $3d5p\ ^1P^o$ intermediate-state autoionizing resonance. The $3d5p\ ^1P^o$ resonance is the broad structure stretching from $\omega\sim0.237$ to 0.247 a.u. The superimposed sharp structures are due to final-state autoionizing resonances attached to the $4d$ threshold at ~0.242 a.u. and to the $5p$ threshold at ~0.250 a.u.

shape very well; 20 Å to the blue of the peak, the experimental cross section is the same height as the resonance (the $3s3p\ ^1P^o$ intermediate state resonance is to the blue). We did not obtain agreement with the experimental results even after we used experimental energies for our calculated $3s3p\ ^1P^o$ intermediate state and our $3p^2\ ^1S$ resonance in Eq. (1). We do not know the reason for this discrepancy. Moccia and Spizzo [2(b)] have also calculated the two-photon cross section in this energy range. Our cross sections need to be multiplied by the factor $(\omega/\omega_0)4.347\times10^{-18}$ W s, where ω_0 is the atomic unit of frequency, to compare with their results. The two calculated cross sections agree with each other on the whole. Our peak height is 1.6×10^{-45} cm^{4}s, compared with Moccia and Spizzo's height of 1.8×10^{-45} cm^{4}s. The ratio of the peak height near 292 nm to the minimum near 290 nm is 3.2 for our calculation, 2.3 for Moccia and Spizzo, and 1.5 for the experiment. Moccia and Spizzo have calculated the ratio to be 3.8 if only the $3s3p\ ^1P^o$ state is retained in the resolvent, which should be a good approximation. The $3p^2\ ^1S$ resonance played a role in the multiphoton experiments of Hou *et al.* [21]; their fourth photon was in resonance with this state.

In Figs. 4–6 we plot the two-photon ionization cross section of Ca. The spectrum plotted in Fig. 4 is much more interesting than that plotted in Fig. 1; we expect the two-photon cross section for Ba to be the most interesting of the alkaline earths. The Rydberg series attached to the threshold at $\omega\sim0.22$ a.u. is from the $4snp\ ^1P^o$ intermediate-state resonances. The Rydberg series attached to the threshold at ~0.143 a.u. are from two-photon absorption to states of $4pnp$ and $4pnf$ character. The Rydberg series attached to the threshold at ~0.17 a.u. are from two-photon absorption to states of $3dns$ and $3dnd$ character. The cross section is dropping strongly at the two-photon ionization threshold because the $4s4p\ ^1P^o$ state is nearly in resonance at threshold. In Fig. 5 we show a blowup of the frequency region near the two-photon ionization threshold. There are three clear autionizing series attached to the $3d$ threshold; they have the character $3dnd\ ^1S$ (solid line), $3dns\ ^1D$, and $3dnd\ ^1D$. The intensities of these states are magnified by the intermediate state resonance $4s4p\ ^1P^o$ at $\omega\sim0.108$ a.u., and accordingly it may be possible to experimentally observe these resonances. The quantum defect for the $3dnd\ ^1S$ states varies strongly due to the presence of a $4pnp\ ^1S$ perturber near 0.139 a.u. It is easy to see from Fig. 5 that the relative positions of the ^1S and ^1D Rydberg states change near threshold. The effective quantum number $(n-\mu)$ for the ^1S states near 0.122, 0.130, 0.134, and 0.136 a.u. are 3.45, 4.39, 5.27, and 5.98. In Fig. 6 we show the two-photon cross section near the lowest *intermediate-state* autoionizing resonance ($3d5p\ ^1P^o$); the $3d5p\ ^1P^o$ resonance is the broad structure stretching from $\omega\sim0.237$ to 0.247 a.u. There are several final-state autoionizing Rydberg series superimposed on this structure; they are attached to the $4d$ threshold at ~0.242 a.u. and to the $5p$ threshold at ~0.250 a.u. We do not think that this structure will ever be observed experimentally because of the high frequency needed to reach it and its small cross section. However, we are encouraged by this calculation to hope that it will be possible to observe enhancement of the two-photon ionization cross section in a more favorably placed autoionizing state in a different atom or ion. An autoionizing state can be considered a bound state embedded in a continuum (call it continuum 1); by assuming that the dipole matrix element connecting this bound state to the higher continua is much larger than the dipole matrix element connecting continuum 1 to the higher continua, one can show that *all* intermediate state autoionizing resonances connected optically to the initial state will contribute *peaks* to the two-photon cross section independent of their profiles in the one-photon cross section. However, window resonances in the one-photon cross section will probably not enhance the two-photon cross section nearly as much as resonant peaks in the one-photon cross section.

GENERALIZED MQDT

We have described two-photon processes for the interaction of a laser field with a neutral atom. However, the generalized version of MQDT allows the immediate application of the methods described above to *any* dynamic system for which the wave function is known analytically. We can study multiphoton processes for positive or negative ions, for neutral or ionic species in electric fields, for molecules, and for intermediate-Z atoms with non-negligible spin-orbit interactions.

HIGHER-ORDER PROCESSES

The application of this method to higher-order processes should be straightforward. For example, the third-order transition matrix element to go from state Ψ_0 to state Ψ_f is written as [22] $T^{(3)}_{f\leftarrow0}=\langle\Psi_f|D|\Lambda^{(2)}_p\rangle$ with $\Lambda^{(2)}_p$ the solution of the inhomogeneous equation

$$(E_2-H)\Lambda^{(2)}_p=D\Lambda^{(1)}_p \tag{37}$$

and with $\Lambda^{(1)}_p$ the solution of the inhomogeneous equation

$$(E_1-H)\Lambda_p^{(1)}=D\Psi_0\ , \tag{38}$$

where $E_2=E_0+2\omega$ and $E_1=E_0+\omega$. Both $\Lambda_p^{(i)}$ are finite everywhere and have only outgoing waves in the open channels. However, unlike two-photon processes the frequency range over which the method we have described will work is limited. Namely, the frequency cannot be greater than that needed by one photon to excite an electron out of the ground state to distances larger than r_c; the method we have described cannot be used when $\Lambda_p^{(1)}$ in Eq. (37) extends outside the R-matrix box. For neutral species this restricts the photon frequency to less than approximately 5 eV for three-photon processes. We feel that the method outlined in Ref. [23] can possibly be adapted to handle this difficulty.

This iterative procedure can be applied to even-higher-order processes. In practice we only expect reasonable accuracy up to at *most* fourth-order processes due to accumulation of errors. For example, the errors in $\Lambda_p^{(1)}$ are passed through Eq. (37) to $\Lambda_p^{(2)}$. A variational method which used the $\Lambda_p^{(i)}$ to calculate the nth-order matrix element would greatly increase the accuracy of high-order matrix elements. However, generalizing Ref. [24] to multielectron atoms has not yet been accomplished.

CONCLUSIONS

We have presented the tools which would allow a perturbative calculation of two-photon processes. The method uses a variant of the eigenchannel R-matrix procedure to solve for the short-range dynamics by brute force. We match this brute-force solution to Coulomb functions and use a variant of MQDT [11] to solve for the dynamics outside of the reaction zone. We have applied this method to the calculation of the two-photon ionization cross section of Mg and Ca. We have made a realistic calculation of the effect of an intermediate-state autoionizing resonance (Fig. 6) on the two-photon ionization cross section. By using MQDT it is possible to solve for the two-photon dynamics in any of the long-range fields for which the generalized version of MQDT has already been applied (in one-photon processes).

ACKNOWLEDGMENTS

We would like to thank C. H. Greene for reading this manuscript and for helpful discussions related to this work. F.R. is supported by the Division of Chemical Sciences, Office of Basic Energy Sciences, Office of Energy Research, U.S. Department of Energy under Grant No. DE-FG02-90ER14145 and B.G. is supported by NSF Grant No. PHY90-12244.

[1] A. L'Huillier and G. Wendin, Phys. Rev. A **36**, 4747 (1987).
[2] (a) R. Moccia and P. Spizzo, J. Phys. B **18**, 3537 (1985); **21**, 1145 (1988); (b) Phys. Rev. A **39**, 3855 (1989).
[3] H. Bachau and P. Lambropoulos, Z. Phys. D **115**, 37 (1989).
[4] X. Tang, T. N. Chang, P. Lambropoulos, S. Fournier, and L. F. DiMauro, Phys. Rev. A **41**, 5265 (1990); T. N. Chang and X. Tang, *ibid.* **46**, R2209 (1992).
[5] C. Pan, B. Gao, and A. F. Starace, Phys. Rev. A **41**, 6271 (1990).
[6] C. Pan and A. F. Starace, Phys. Rev. A **44**, 324 (1991).
[7] A. F. Starace and T. F. Jiang, Phys. Rev. A **36**, 1705 (1987).
[8] M. G. J. Fink and W. R. Johnson, Phys. Rev. A **42**, 3801 (1990).
[9] H. Bachau, P. Lambropoulos, and X. Tang, Phys. Rev. A **42**, 5801 (1990).
[10] P. Shorer, J. Phys. B **13**, 2921 (1980); P. Shorer and K. T. Taylor, *ibid.* **14**, 4007 (1981); M. T. Smith, K. T. Taylor, and C. W. Clark, in *Proceedings of the Sixteenth International Conference on the Physics of Electronic and Atomic Collisions: Abstracts of Contributed Papers,* edited by A. Dalgarno, R. S. Freund, M. S. Lubell, and T. B. Lucatorto (XVI ICPEAC Program Committee, New York, 1989), p. 99.
[11] M. G. J. Fink and P. Zoller, Phys. Rev. A **39**, 2933 (1989).
[12] C. H. Greene, Phys. Rev. A **32**, 1880 (1985); C. H. Greene and M. Aymar, *ibid.* **44**, 1773 (1991), and references therein.
[13] F. Robicheaux and Bo Gao, Phys. Rev. Lett. **67**, 3066 (1991).
[14] A. Dalgarno and J. T. Lewis, Proc. R. Soc. London Ser. A **233**, 70 (1955).
[15] U. Fano and A. R. P. Rau, *Atomic Collisions and Spectra* (Academic, Orlando, 1986); M. J. Seaton, Rep. Prog. Phys. **46**, 167 (1983).
[16] C. H. Greene and L. Kim, Phys. Rev. A **36**, 2706 (1987).
[17] A. R. Edmonds, *Angular Momentum in Quantum Mechanics* (Princeton University Press, Princeton, NJ, 1974).
[18] M. D. Lindsay *et al.*, Phys Rev. A **46**, 3789 (1992), and references therein.
[19] U. Fano, Phys. Rev. A **32**, 617 (1985).
[20] R. E. Bonanno, C. W. Clark, and T. B. Lucatorto, Phys. Rev. A **34**, 2082 (1986).
[21] M. Hou, P. Breger, G. Petite, and P. Agostini, J. Phys. B **23**, L583 (1990).
[22] Y. Gontier and M. Trahin, Phys. Rev. **172**, 83 (1968).
[23] C. W. Clark, J. Opt. Soc. Am. B **7**, 488 (1990).
[24] Bo Gao and A. F. Starace, Phys. Rev. Lett. **61**, 404 (1988); Phys. Rev. A **39**, 4550 (1989).